

Cloud, Aerosol, and Complex Terrain Interactions (CACTI) ARM Aerial Facility (AAF) Measurements of Ice Nucleating Particles Field Campaign Report

P DeMott

T Hill

April 2020



DISCLAIMER

This report was prepared as an account of work sponsored by the U.S. Government. Neither the United States nor any agency thereof, nor any of their employees, makes any warranty, express or implied, or assumes any legal liability or responsibility for the accuracy, completeness, or usefulness of any information, apparatus, product, or process disclosed, or represents that its use would not infringe privately owned rights. Reference herein to any specific commercial product, process, or service by trade name, trademark, manufacturer, or otherwise, does not necessarily constitute or imply its endorsement, recommendation, or favoring by the U.S. Government or any agency thereof. The views and opinions of authors expressed herein do not necessarily state or reflect those of the U.S. Government or any agency thereof.

**Cloud, Aerosol, and Complex Terrain
Interactions (CACTI) ARM Aerial Facility
(AAF) Measurements of Ice Nucleating
Particles Field Campaign Report**

P DeMott
T Hill
Both at Colorado State University

April 2020

Work supported by the U.S. Department of Energy,
Office of Science, Office of Biological and Environmental Research

Acronyms and Abbreviations

AAF	ARM Aerial Facility
AMF	ARM Mobile Facility
ARM	Atmospheric Radiation Measurement
CACTI	Cloud, Aerosol, and Complex Terrain Interactions
CSU	Colorado State University
DI	deionized
G-1	Gulfstream-159 aircraft
INP	ice nucleating particle
IS	ice spectrometer
PCR	polymerase chain reaction
SL	standard liters

Contents

Acronyms and Abbreviations	iii
1.0 Summary.....	1
2.0 Results	4
3.0 Publications and References	8

Figures

1 Filter sampler on the G-1 aircraft.....	3
2 INP number per filter for all unamended samples and blanks, and the average fit used to correct data over the study period.....	3
3 Ice nucleating particle number concentrations versus processing temperature for all samples from the AAF G-1 sampling period (November to December 2018), corrected for filter blanks.....	6
4 Comparison of AMF1 INP filter samples (DeMott et al. 2020) during AAF intensive operations flight period (left) versus AAF flight samples (right), including unamended and heat treatment results.....	7
5 Two specific flight day comparisons to ground-based AMF1 data.....	8

Tables

1 Comparison of the anticipated filter collections to those obtained and processed.....	4
2 List of filter sample metadata for the AAF G-1 CACTI campaign, including altitude and fractional latitude and longitude at the start and stop of each leg (a filter collection period), and the standard liter volume (SL) collected per leg and total (multiple legs constituted some filters).....	5

1.0 Summary

During the Cloud, Aerosol, and Complex Terrain Interactions (CACTI) Experiment, a project with the overarching goal to improve understanding of cloud life cycle and organization in relation to environmental conditions so that cumulus, microphysics, and aerosol parameterizations in multi-scale models can be improved, our group was tasked with providing and assisting the collection of aerosol filter samples for measuring ice nucleating particle (INP) concentrations. This included ground-based and aircraft measurements. This report details the efforts and results from the Atmospheric Radiation Measurement (ARM) Aerial Facility (AAF) Gulfstream-159 (G-1) aircraft.

The INP measurements were especially focused around research needs for addressing the major CACTI science questions regarding the role of aerosols as one factor affecting the properties and life cycles of orographically generated cumuli, and the initiation of deep convection and mesoscale organization. As the primary means for first initiation of the ice phase in clouds, absent remnant ice particles from prior convection or overseeding from higher clouds (cirrus) where homogeneous freezing can occur, the abundance of INPs can play a powerful role in the formation of precipitation. The INP data collected may ultimately be related in future investigations to other G-1 measurements of aerosol properties and location with respect to storm systems. This data can serve as the basis for developing and improving numerical model parameterizations of ice nucleation.

Within efforts to measure INPs in CACTI, the AAF G-1 measurements provided the unique ability to capture INPs above the surface layer, in both inflow and cold pool regions around storms that were also penetrated for cloud property measurements. CACTI INP measurements on the G-1 were collected from varied altitudes on different flights over the region of the Sierras de Córdoba mountain range of north central Argentina. Within this region, a vast array of aerosol influences was expected to be encountered, from local soil and plant emissions, long range transported desert dusts, regional pollution, and even biomass burning. Twenty-two research flights were conducted from November 4 to December 8, 2018.

This report describes the installation, collections, processing, and archiving of data from this effort. A filter sampling system was deployed on the G-1 to collect aerosol particles for post-processing for measuring their immersion freezing ability once returned to Colorado State University (CSU). Images of the filter sampler system installed in a rack tray on the G-1 are shown in Figure 1. This configuration mimics that used by Levin et al. (2019). Filter holders were 47-mm anodized aluminum in-line units (Pall). Pre-cleaned (to remove any INPs present after manufacture) and pre-sterilized (to remove any biologically active material) Nuclepore polycarbonate filters (0.2- μm pore size, backed by clean 10- μm pore size filters) were provided wrapped in aluminum pouches and double-bagged for transport to Argentina, and use in the in-line holders. The holders were loaded pre-flight, and used holders were also cleaned/sterilized after each use. Dr. Thomas Hill coordinated the first three weeks of collections during the intensive operational period, and trained Department of Energy personnel (Lexie Goldberger, Mikhail Pekour, and Kaitlyn Suski) to complete sampling until the end of the campaign. Filters were drawn for varied times, resulting in varied volumes collected. Mass flow rate was recorded (Figure 1) in real-time so that total sampled volume (at standard temperature and pressure) could be determined for each filter. A total of 34 sample filters were collected over the intensive operational period, as listed in Table 1, including five blanks (installed with no flow) at intervals throughout the project. Filters were stored

temporarily in parafilm-sealed petri dishes in a -20°C freezer prior to return to CSU at the end of the campaign with a dry nitrogen shipper (Cryoport.com).

Initial processing to obtain spectra of INP number concentration active via the immersion freezing mechanism versus temperature was conducted using the CSU ice spectrometer (IS) instrument system (McCluskey et al. 2018). For processing, each filter was placed into a 50 mL Falcon polypropylene centrifuge tube with 7 mL of $0.1\ \mu\text{m}$ -filtered deionized (DI) water and shaken in a Roto-Torque rotator for 20 min to create a suspension. Thirty-two aliquots of $50\ \mu\text{L}$ (i.e., 1.6 mL) of each sample, plus a series of dilutions, were then dispensed into polymerase chain reaction (PCR) trays that were then fitted into aluminum blocks in the IS. Samples were cooled at a rate of approximately $0.33^{\circ}\text{C}\ \text{min}^{-1}$. Freezing temperatures of wells were recorded using a camera and software system on each of three IS instrument systems. The lowest freezing temperature archived for each sample was defined by the temperature for which the number of sample wells frozen significantly exceeded those frozen in a 32-well, $0.02\ \mu\text{m}$ -filtered DI water blank tested simultaneously in the same tray. This final temperature was generally between -26 and -29°C for the CACTI AAF sample set. Cumulative INP concentrations were determined by first calculating the INPs per mL of suspension based on Vali (1971) and then converting to concentration per standard liter of air using the proportion of the total liquid sample dispensed and the air sample volumes. The number of INPs on the average of all blank filters that had been handled and processed identically, with exception of air flow, were subtracted from the calculated number of INPs on each sample filter (Figure 2) before the conversion to number concentration per standard liter. While the numbers of INPs collected on filters significantly exceeded blank filter background numbers at most times, increasing the limited sample volumes possible in the aircraft sampling configuration used in CACTI remains as a future need. Confidence intervals (95%) for binomial sampling were calculated based on Agresti and Coull (1998).

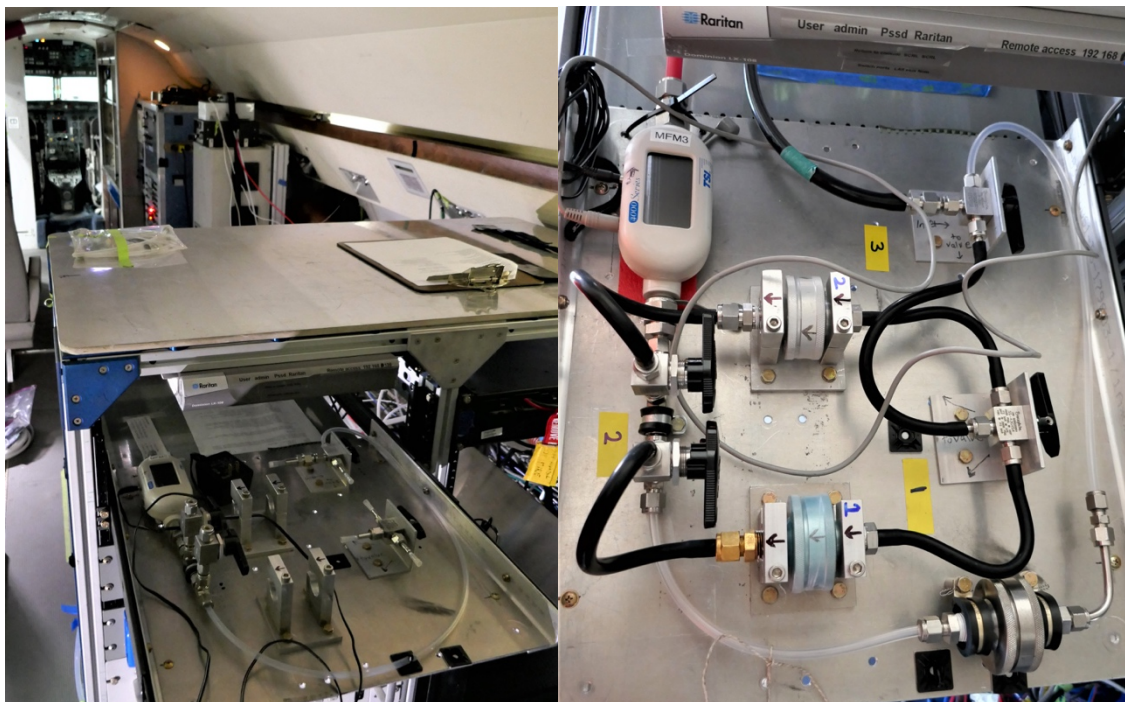


Figure 1. Filter sampler on the G-1 aircraft. Two filters could be loaded at any time into anodized aluminum or stainless steel holders (Pall), and sequentially sampled through the use of switching ball valves during flight. Airflow entered from the G-1 isokinetic inlet into interior 3/8-inch conductive tubing (2-m length), and through the flowmeter shown in the upper left of the righthand figure before passing to either filter (typically one for above and one for below cloud sampling). Mass flow rate was recorded at 1 Hz. When filters were not being sampled, a bypass flow (plastic line to “dummy” filter) was run. A LabView program was used to monitor the mass flow rate, temperature, and pressure, so that volume flow rate at standard conditions could be calculated, and integrated sample volume determined.

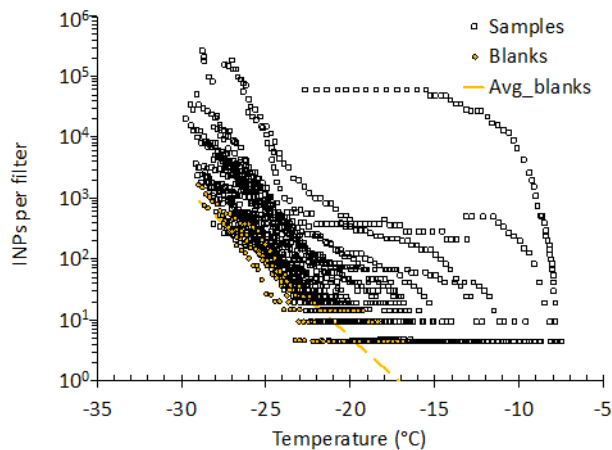


Figure 2. INP number per filter for all unamended samples and blanks, and the average fit used to correct data over the study period.

To gain insights into the biological proportion of INPs, a portion of a selected number of original suspensions was heated to 95°C for 20 min, prior to determining the immersion freezing temperature spectra. This thermal treatment should denature most heat-labile organics, such as proteins. Hydrogen peroxide (H₂O₂) digestions were also performed on portions of suspensions for selected samples to remove all organic carbon INPs following methods detailed in McCluskey et al. (2018) and Suski et al. (2018). This was typically done for the same filter samples for which thermal treatments were done. The peroxide treatment is also done at 95°C, thus incrementally removing all remaining organics. The difference in the INP concentrations versus temperature after heat or peroxide treatment determines the contributions of biological and organic INP types, respectively, for each filter sample period. For archival and completion of tasks under this ARM proposal, all 34 original filter particle collections were processed for basic temperature spectra, with 13 of these 34 also tested for thermally removing microbial/proteinaceous contributions toward INPs, and 10 also treated to remove of all organic carbon (Table 1); more samples were heat treated because it was found that heat alone typically reduced INPs to near-background levels Metadata for processed filters is shown in Table 2. All data have been added to the ARM Data Center.

Table 1. Comparison of the anticipated filter collections to those obtained and processed.

Campaign	Base	Blanks	95 C	H₂O₂	Processes
CACTI AAF Anticipated	60				
Promised	60		12*	12*	
Obtained	34	5			
<i>Processed</i>	34	5	13	10	62

* = promised processing of 1/3 of total collected

2.0 Results

Results are at an early stage of evaluation, as final processing was completed just prior to the drafting of this report. Some first results are shown in Figures 3 to 5. In Figure 3, all flight data and all INP processing condition data are shown as a function of processing temperature. The results indicate the presence aloft at times of apparent biological INPs, removed with thermal processing, with a special role in accounting for not only most immersion freezing INPs active in the temperature regime higher than ~ -17°C (Figure 3), but also often to much colder temperatures (not apparent in this composite figure). These biological INPs are largely responsible for the “hump” in INP activity that leads the INP spectra to diverge positively from exponential at these higher temperatures, consistent with other reports attributing such impact to this category of INPs (Hill et al. 2018, O’Sullivan et al. 2018). Other organic entities typically contribute the bulk of INPs below -23°C and were (surprisingly) dominant over inorganic INPs (presumed as those left after peroxide treatments of suspensions) in that temperature range. The INP spectra of the inorganic populations of INPs, indicated by the INPs remaining after H₂O₂ treatments in Figure 3, are highly exponential versus temperature, with an approximate 1 order of magnitude increase in atmospheric concentrations for each 4°C of cooling. The temperature spectra, represented by the $\Delta[\text{INP}]/dT$ following treatments, are remarkably consistent with laboratory measurements made on Argentinian soil dust from La Pampa province, the province just south of Córdoba province, reported by DeMott et al. (2018). These same results were noted in the first ARM Mobile Facility (AMF1) measurement record (DeMott et al. 2020), as discussed later.

Table 2. List of filter sample metadata for the AAF G-1 CACTI campaign, including altitude and fractional latitude and longitude at the start and stop of each leg (a filter collection period), and the standard liter volume (SL) collected per leg and total (multiple legs constituted some filters).

Start day	Start month	Start year	RF No.	Leg	Start time (UTC)	Start latitude	Start longitude	Start altitude (m)	Stop time (UTC)	Stop latitude	Stop longitude	Stop altitude (m)	Leg SL (1013 hPa, 273 K)	Total SL (1013 hPa, 273 K)	Type	
6	11	2018	2	1	15:11:21	-32.21133	-64.91508	5724.4	15:35:22	-32.02121	-64.74758	2500.3	182.8			
6	11	2018	2	2	16:00:15	-32.21453	-65.09025	1682.2	16:07:22	-31.97230	-65.10403	1353.6	83.3	266.0	Below cloud Blank	
10	11	2018	3	1	12:35:22	-32.18914	-64.74392	2381.2	13:42:52	-32.40457	-65.10541	3700.8	553.2	553.2	Above cloud	
10	11	2018	3	2	1	13:48:38	-32.45422	-65.14573	1790.1	14:01:58	-31.85073	-65.10229	1759.8	135.9		Below cloud
				2	14:53:50	-31.85015	-64.74895	2591.0	14:57:31	-32.04902	-64.71306	2308.9	34.8	170.7	Below cloud	
12	11	2018	4	1	17:27:11	-31.97407	-64.92657	3352.5	17:46:06	-31.83609	-64.69260	2417.4	159.9		Above cloud	
12	11	2018	4	2	1	17:49:18	-31.99638	-64.74927	2198.3	18:09:40	-32.36651	-64.92567	3330.4	183.1	343.0	Above cloud
				2	18:43:18	-32.40366	-65.11016	1261.8	18:51:57	-31.89935	-65.10633	1254.7	105.0	105.0	Below cloud	
14	11	2018	5	1	14:17:09	-32.88336	-64.52911	2874.2	17:36:47	-32.53067	-64.70702	3299.3	1570.6	1570.6	Clear air	
14	11	2018	5	2	-	-	-	-	-	-	-	-	-	-	Blank	
15	11	2018	6	1	13:13:33	-32.85679	-64.57030	2318.6	15:36:12	-32.48554	-64.66909	2228.0	1389.6	1389.6	Clear air	
16	11	2018	7	1	14:35:24	-32.35830	-64.74367	1559.3	14:42:08	-32.11522	-64.74929	1965.5	69.1		Below cloud/clear air	
				2	14:46:53	-32.39887	-64.72894	2064.4	15:33:15	-32.38299	-64.90659	3436.0	386.7	455.8	Below cloud/clear air	
17	11	2018	8	1	12:44:46	-32.28419	-65.10967	1942.1	12:54:58	-31.81421	-65.10151	2225.4	107.3		Below cloud	
				2	13:47:22	-31.91919	-64.72114	2705.3	13:55:29	-32.38936	-64.69919	2703.7	77.1		Below cloud	
				3	15:18:39	-32.25082	-64.71779	2286.3	15:25:42	-31.84839	-64.72067	2216.1	72.2	256.7	Below cloud	
20	11	2018	9	1	16:46:22	-32.43739	-65.10998	1282.5	17:11:09	-32.45374	-65.13042	2191.1	263.6	263.6	Below cloud/clear air	
20	11	2018	9	2	1	18:01:13	-32.37606	-64.91571	4010.1	18:10:39	-31.84587	-64.92447	4507.2	74.4	74.4	Above cloud
21	11	2018	10	1	18:45:11	-32.22132	-64.71639	2587.3	18:53:10	-31.81116	-64.63630	2931.6	72.2	72.2	Below cloud	
21	11	2018	10	2	-	-	-	-	-	-	-	-	-	-	Blank	
22	11	2018	11	1	15:32:49	-31.94365	-64.71620	2830.8	15:47:19	-32.21077	-64.71509	2720.7	145.7		Between layers	
				2	17:12:38	-31.89647	-64.71824	4266.7	17:22:23	-32.42264	-64.64513	3913.3	80.5	226.2	Between layers	
22	11	2018	11	2	1	16:03:49	-32.19455	-64.71583	1561.0	16:15:07	-32.10880	-64.73921	1745.3	105.7		Below cloud
				2	17:37:46	-31.89091	-64.71097	2155.3	17:47:35	-32.39273	-64.71107	1672.4	89.9	195.6	Below cloud	
24	11	2018	12	1	16:48:58	-32.15203	-64.75927	1578.9	17:22:22	-31.83934	-64.71533	2253.4	327.7	327.7	Below cloud	
24	11	2018	12	2	1	19:50:03	-31.77650	-64.67577	2318.9	20:01:14	-32.41867	-64.69834	2325.5	115.7	115.7	Below cloud
25	11	2018	13	1	16:17:54	-32.09240	-64.73722	2862.3	16:44:41	-31.80441	-64.70287	2882.3	174.2	174.2	Below cloud	
25	11	2018	13	2	1	18:26:36	-32.11219	-64.71995	2575.4	18:44:33	-32.12313	-64.71853	2349.2	184.4	184.4	Below cloud
28	11	2018	14	1	15:36:19	-32.12040	-64.74030	1675.0	15:59:44	-32.41310	-64.70400	1857.0	252.0	252.0	Below cloud	
28	11	2018	14	2	1	17:00:34	-32.40570	-65.11950	3224.0	17:24:36	-32.22220	-65.03620	3054.0	245.5	245.5	Clear air profile
29	11	2018	15	1	14:45:12	-32.11816	-64.76373	1673.0	14:54:39	-32.37263	-64.73439	2587.0	105.6	105.6	Below cloud	
29	11	2018	15	2	1	15:58:25	-32.23359	-64.71485	2027.9	16:18:09	-32.49981	-64.51640	2005.7	199.7	199.7	Below cloud
1	12	2018	16	1	1	18:06:17	-31.91953	-64.71538	3200.3	18:38:09	-32.73367	-64.43026	2128.2	312.9	312.9	Between layers
1	12	2018	16	2	-	-	-	-	-	-	-	-	-	-	Blank	
2	12	2018	17	1	1	15:06:24	-31.78860	-64.65550	2898.0	15:17:11	-32.36060	-64.71380	2897.0	103.2	103.2	Above cloud
2	12	2018	17	2	1	15:27:11	-32.34880	-64.68880	4586.0	15:35:13	-31.85000	-64.71520	4552.0	62.8	62.8	Above cloud
3	12	2018	18	1	1	16:32:39	-32.10455	-64.73497	1595.6	17:10:14	-32.43625	-64.78689	3343.8	336.0	336.0	Below cloud
3	12	2018	18	2	1	18:28:51	-32.17772	-64.79398	3342.7	19:19:50	-31.84991	-64.99249	3329.6	428.3	428.3	Above cloud
4	12	2018	19	1	1	18:34:32	-32.30410	-64.70303	3325.2	18:40:42	-32.15457	-64.87276	3537.7	51.3	51.3	Below cloud
4	12	2018	19	2	1	19:15:01	-32.34629	-64.92248	3671.5	19:29:31	-32.56339	-64.72018	3663.7	120.7	120.7	Below cloud
5	12	2018	20	1	1	12:38:40	-31.78460	-64.65598	6236.2	12:56:09	-32.08061	-64.73116	6035.8	106.5	106.5	Above cloud
5	12	2018	20	2	1	14:42:22	-32.38212	-64.72829	2380.3	14:54:39	-31.88951	-64.71431	2034.5	127.2	127.2	Below cloud
7	12	2018	21	1	1	15:32:57	-32.23972	-64.72219	1641.7	15:44:08	-32.10182	-64.71991	2124.9	109.7		Below cloud
				2	16:02:16	-32.44209	-64.65562	2957.1	16:12:56	-31.88133	-64.71802	3406.7	85.3		Above cloud	
				3	16:35:20	-32.02982	-64.72033	2434.0	16:45:10	-32.04993	-64.71638	2226.1	90.6		Below cloud	
				4	18:08:26	-32.41625	-64.67908	2311.3	18:25:11	-31.89865	-64.71647	2764.3	153.2		Below cloud	
				5	18:37:15	-32.29837	-64.72101	1636.2	18:53:06	-32.73273	-64.50075	1644.5	160.0	598.9	Below cloud	
7	12	2018	21	2	1	17:17:51	-32.40716	-64.66961	3297.8	17:28:08	-31.92904	-64.71931	3715.7	87.7	87.7	Above cloud
8	12	2018	22	1	1	16:26:33	-32.37527	-64.86849	3332.0	19:16:24	-32.61694	-64.57518	1545.2	1667.2	1667.2	Clear air
8	12	2018	22	2	-	-	-	-	-	-	-	-	-	-	Blank	

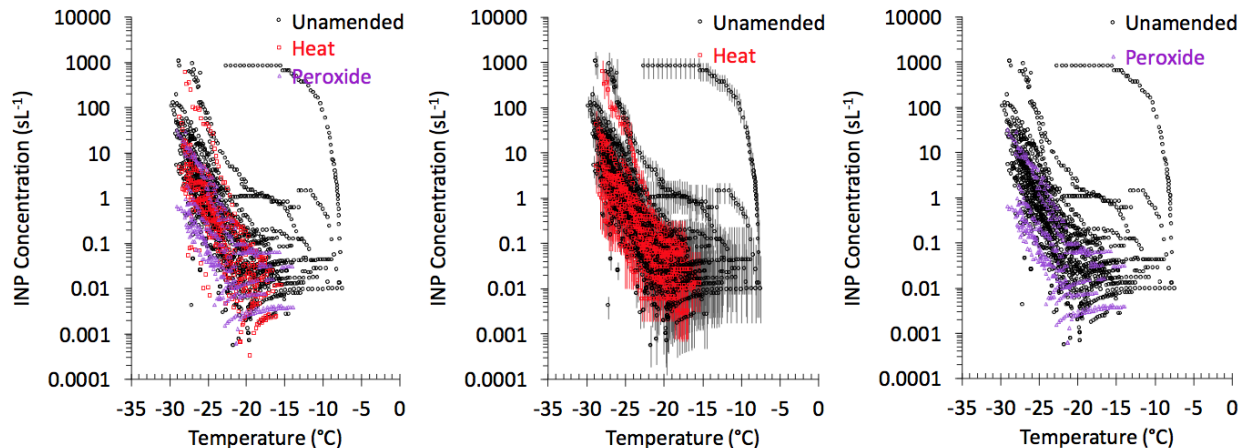


Figure 3. Ice nucleating particle number concentrations versus processing temperature for all samples from the AAF G-1 sampling period (November to December 2018), corrected for filter blanks. From left to right are all processes, unamended and thermally treated (95°C) only, and unamended and H₂O₂-treated only processes. Uncertainties are shown only for the middle panel. Results show the moderate presence of biological and organic INPs, especially dominant at temperatures higher than about -17°C.

One striking result shown in Figure 3 is from the filter collected in the boundary layer during Research Flight 10, with INP concentrations of several hundred per standard liter evident at -15°C. No special event, or real or potential artifact, was noted in the flight notes for this collection, so the high INP concentration for this boundary-layer flight period is still under investigation. The nature of the spectra, rising to a plateau, is suggestive of the influence by a single INP type, such as might be expected for capturing airborne pollen on the filter, which could then burst within the liquid suspension to create additional INPs (Pummer et al. 2012). However, the only previous investigation of pollen impacts on boundary-layer INPs found very modest increases in average INP concentrations during high-pollen periods, and only one event of INPs increasing to 30 sL⁻¹ at -20°C following a heavy rain event, leading the authors to conclude that such bursting release of macromolecular INPs from pollen was “not prevalent for the pollen types and meteorological conditions typically encountered in the southeastern US” (Hader et al. 2014). Presently, the results are considered valid for now, triggered by an unusual INP event.

A comparison of AMF1 and AAF CACTI results is shown in Figure 4, for the unamended and thermally treated samples only, to demonstrate the relative consistency between the two data sets, the resolution of which is only limited by the much lower sample volumes for the AAF samples (note the higher uncertainties in the regime > -20°C for the AAF data). Nevertheless, even without intercomparing on a daily basis, it is evident that the concentration ranges and heat impacts at the higher temperature end are consistent between the data sets.

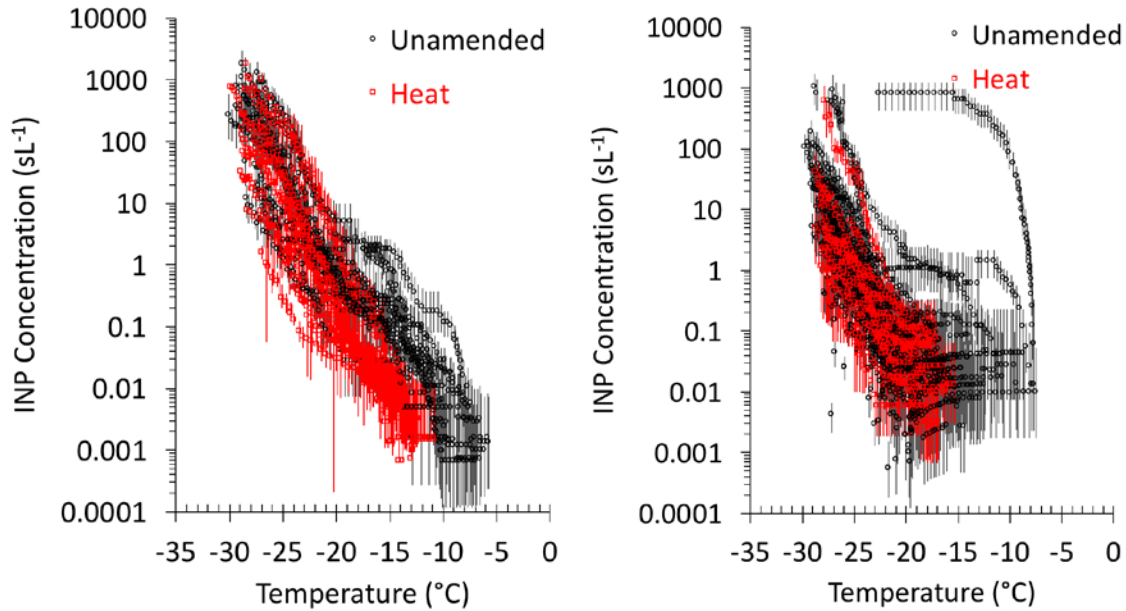


Figure 4. Comparison of AMF1 INP filter samples (DeMott et al. 2020) during AAF intensive operations flight period (left) versus AAF flight samples (right), including unamended and heat treatment results. Higher-volume samples at the AMF site allow for wider dynamic measurement range, while AAF filters include both sub-cloud boundary layer and samples from above clouds in the mid-troposphere.

Finally, in Figure 5, results from two days are shown to compare INP temperature spectra obtained on the G-1 versus at the AMF1 site during the general time of overflight periods. On both days, the spectral shapes are similar at the surface and aloft, and the impact of biological INPs is indicated across a broad temperature range by the loss of activity with heating to 95°C. The November 12 case, a day of deeper convection and heavy rain in the area, suggests a well-mixed boundary layer, with near perfect correspondence of unamended and heated AAF and AMF samples over the more limited sensitivity range of the lower-volume AAF samples. This was the case for a number of days, but also many days reflected a greater decrease of INPs at higher altitude than could be explained by correction to standard liters. Hence, at other times, as on November 17, the boundary layer appears to have been decoupled from the sub-cloud layer, or there were additional factors that led to the dilution of air aloft and closer to cloud base. In general, above-cloud samples reflected the lowest INPs (not shown).

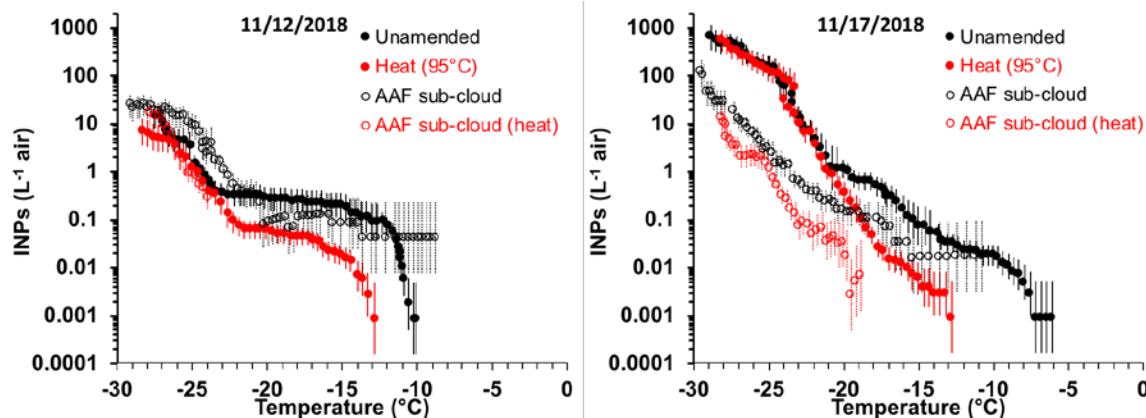


Figure 5. Two specific flight day comparisons to ground-based AMF1 data. November 12 was a day of deep convection and heavy rain, showing an excellent comparison of ground-based versus sub-cloud INPs. November 17 was a drier and dustier day at the surface, but with a clear decoupling/dilution of air in the boundary layer compared to the surface, where local soil emissions were enhanced.

3.0 Publications and References

No publications have been prepared at the time of this report. First presentation of results is planned to occur at the Department of Energy ARM/Atmospheric System Research Principal Investigators meeting in June 2020. Publications are in preparation, and advanced analyses have been proposed at the time of this report. References follow.

Agresti, A, and BA Coull. 1998. “Approximate is better than ‘exact’ for interval estimation of binomial proportions.” *The American Statistician* 52(2): 119–126, <https://doi.org/10.1080/00031305.1998.10480550>

DeMott, P, and T Hill. 2020. Cloud, Aerosol, and Complex Terrain Interactions (CACTI) ARM Mobile Facility (AMF) Measurements of Ice Nucleating Particles Field Campaign Report. U.S. Department of Energy. DOE/SC-ARM-20-006.

DeMott, PJ, O Möhler, DJ Cziczo, N Hiranuma, MD Petters, SS Petters, F Belosi, HG Bingemer, SD Brooks, C Budke, M Burkert-Kohn, KN Collier, A Danielczok, O Eppers, L Felgitsch, S Garimella, H Grothe, P Herenz, TCJ Hill, K Höhler, ZA Kanji, A Kiselev, T Koop, TB Kristensen, K Krüger, G Kulkarni, EJT Levin, BJ Murray, A Nicosia, D O’Sullivan, A Peckhaus, MJ Polen, HC Price, N Reicher, DA Rothenberg, Y Rudich, G Santachiara, T Schiebel, J Schrod, TM Seifried, F Stratmann, RC Sullivan, KJ Suski, M Szakáll, HP Taylor, R Ullrich, J Vergara-Temprado, R Wagner, TF Whale, D Weber, A Welti, TW Wilson, MJ Wolf, and J Zenker. 2018. “The Fifth International Workshop on Ice Nucleation phase 2 (FIN-02): laboratory intercomparison of ice nucleation measurements.” *Atmospheric Measurement Techniques* 11(11): 6231–6257, <https://doi.org/10.5194/amt-11-6231-2018>

Hader, JD, TP Wright, and MD Petters. 2014. “Contribution of pollen to atmospheric ice nuclei concentrations.” *Atmospheric Chemistry and Physics* 14(11): 5433–5449, <https://doi.org/10.5194/acp-14-5433-2014>

Hill, TCJ, PJ DeMott, F Conen, and O Möhler. 2018. “Impacts of bioaerosols on atmospheric ice nucleation processes.” in Delort, A-M, and P Amato, eds. *Microbiology of Aerosols*. John Wiley & Sons, Hoboken, New Jersey, ISBN 97781119132288.

Levin, EJT, PJ DeMott, KJ Suski, Y Boose, TCJ Hill, CS McCluskey, GP Schill, K Rocci, H Al-Mashat, LJ Kristensen, GC Cornwell, KA Prather, JM Tomlinson, F Mei, J Hubbe, MS Pekour, RJ Sullivan, LR Leung, and SM Kreidenweis. 2019. “Characteristics of ice nucleating particles in and around California winter storms.” *Journal of Geophysical Research – Atmospheres* 124(21): 11,530-11,551, <https://doi.org/10.1029/2019JD030831>

McCluskey, CS, J Ovadnevaite, M Rinaldi, J Atkinson, F Belosi, D Ceburnis, S Marullo, TCJ Hill, U Lohmann, ZA Kanji, C O’Dowd, SM Kreidenweis, and PJ DeMott. 2018. “Marine and Terrestrial Organic Ice Nucleating Particles in Pristine Marine to Continentally-Influenced Northeast Atlantic Air Masses.” *Journal of Geophysical Research – Atmospheres* 123(11): 6196–6212, <https://doi.org/10.1029/2017JD028033>

O’Sullivan, D, MP Adams, MD Tarn, AD Harrison, J Vergara-Temprado, GCE Porter, MA Holden, A Sanchez- Marroquin, F Carotenuto, TF Whale, JB McQuaid, R Walshaw, DHP Hedges, IT Burke, Z Cui, and BJ Murray. 2018. “Contributions of biogenic material to the atmospheric ice-nucleating particle population in North Western Europe.” *Scientific Reports* 8:13821, <https://doi.org/10.1038/s41598-018-31981-7>

Petters, MD, and TP Wright. 2015. “Revisiting ice nucleation from precipitation samples.” *Geophysical Research Letters* 42(20): 8758–66, <https://doi.org/10.1002/2015GL065733>

Pummer, BG, H Bauer, J Bernardi, S Bleicher, and H Grothe. 2012. “Suspendable macromolecules are responsible for ice nucleation activity of birch and conifer pollen.” *Atmospheric Chemistry and Physics* 12(5): 2541–2550, doi:10.5194/acp-12-2541-2012.

Suski, KJ, TCJ Hill, EJT Levin, A Miller, PJ DeMott, and SM Kreidenweis. 2018. “Agricultural harvesting emissions of ice-nucleating particles.” *Atmospheric Chemistry and Physics* 18(18): 13755–13771, <https://doi.org/10.5194/acp-18-13755-2018>

Vali, G. 1971. “Quantitative evaluation of experimental results on the heterogeneous freezing nucleation of supercooled liquids.” *Journal of the Atmospheric Sciences* 28(3): 402–409, [https://doi.org/10.1175/1520-0469\(1971\)028<0402:QEOERA>2.0.CO;2](https://doi.org/10.1175/1520-0469(1971)028<0402:QEOERA>2.0.CO;2)



U.S. DEPARTMENT OF
ENERGY

Office of Science